Springer

KSME

Journal of Mechanical Science and Technology 30 (3) (2016) 1217~1224
www.springerlink.com/content/1738-494x(Print)/1976-3824(Online)
DOI 10.1007/s12206-016-0225-3

Secondary velocity and mixing characteristics of pulsatile flow in small-amplitude sinusoidal vessels †

Minh Tuan Nguyen[1] and Sang-Wook Lee[2,*]

[1]*Department of Mechanical Engineering, The Graduate School, University of Ulsan, Ulsan 44610, Korea*
[2]*School of Mechanical Engineering, University of Ulsan, Ulsan 44610, Korea*

(Manuscript Received August 24, 2015; Revised October 6, 2015; Accepted November 10, 2015)

Abstract

Numerical simulations on pulsatile flow within sinusoidally wavy shaped vessels were conducted for mean Reynolds number of 350, which is in the range of physiological flow rates. We considered the constant pitch of six tube diameters 6D and relatively small amplitudes from A = 0.1D to 0.5D for sinusoidal vessel geometry and investigated the secondary velocity profiles and particle mixing characteristics. The results showed that relatively small amplitude of wavy vessel geometry has significant influence on the nature of flow patterns and particle mixing characteristics. This implies that characterizing accurate geometry is essential for accurate prediction of in vivo hemodynamics and may motivate further study on any possibility of reflection of secondary flow on vascular remodeling and pathophysiology.

Keywords: Small-amplitude sinusoidal vessel; Secondary velocity; Mixing; Pulsatile flow; Computational fluid dynamics

1. Introduction

Since Caro et al. [1] suggested that local blood flow dynamics have controlling effects on atherosclerosis, there has been much evidence showing that the development of cardiovascular diseases such as atherosclerosis and aneurysm are influenced by local hemodynamic environments. In particular, blood flow induced endothelial shear stress, known to be one of the most important hemodynamic factors, has been demonstrated to be strongly correlated with biological responses of vascular system [2].

Many experimental and computational studies on blood flow dynamics have demonstrated that vessel geometry is the primary determinant of hemodynamics [3, 4] explaining the focal nature of atherosclerosis with its predominant occurrence at the bend or the bifurcation.

Although a vessel appears relatively straight in the majority of vascular structure and it is quite common in the literature that wall shear stress is simply estimated based on an assumption of fully developed axisymmetric velocity profile, wavy shaped vessels rather than straight tubes are often observed in *in vivo* vascular systems. Earlier in 1990, Caro et al. [5] imaged the flow in the human common carotid using Phase-contrast magnetic resonance (PC-MR) angiography and showed the development of secondary flow motion by small vessel curvature. Similarly, Ford et al. [6] recently presented that the secondary curvature (minor wiggle) in common carotid artery is not exception, but more common by characterizing the shape and degree of skewing of velocity profile from cine PC-MR images. Myers et al. [7] demonstrated the presence and significance of small-amplitude out-of-plane curvature in a study of blood flow dynamics within human right coronary artery. The observations of these kinds of wavy as well as helical vascular structure have been frequently made in other literatures [8-10].

The small-amplitude wavy geometry may have some clinical implication on endothelial function and the activation of platelet through enhancing particle mixing process induced by secondary flow. A study for mixing effectiveness within helical tubes by Cookson et al. [11] showed that secondary curvature in helical geometries induces significant effect on flow structures and mixing and then may reduce platelet activation and atherosclerosis. But the study considered only steady inflow with constant flow rate in time.

In the present study, we hypothesized the in-plane small-amplitude sinusoidal curvature may induce significant secondary flow and effective mixing, and conducted Computational fluid dynamics (CFD) simulations with various sinusoidally wavy geometries rather than complicate in vivo human vascular geometry. We considered the constant pitch of six tube diameters 6D and relatively small amplitudes for sinusoidal

*Corresponding author. Tel.: +82 52 259 2765, Fax.: +82 52 259 1680
E-mail address: leesw@ulsan.ac.kr
† Recommended by Associate Editor Hyoung-gwon Choi

vessel geometry and pulsatile inflow condition which is intrinsic in cardiovascular flow, based on canonical carotid flow rate waveform [4].

2. Method

2.1 Geometry and boundary conditions

We selected sinusoidal curve formulation for the centerline of vessel geometry (Fig. 1) in three-dimensional space of Cartesian coordinate which can be described as

$$y = A\sin\left(x/c\right) \tag{1}$$

where the wave length or pitch of the curve is $\lambda = 2\pi c = 6D$ and A is the amplitude of the sine curve. Various amplitudes were considered from 0.1D to 0.5D with increments of 0.1D.

The total length of the vessels is five wavelengths (30D). These parameters of vessel configuration basically follow the ones in a study for steady flow in small amplitude helical vessels by Cookson et al. [11]. The minimum radius of curvature with the amplitude of 0.5D corresponds to ~2D. Meyers et al. [7] reported the presence of significant secondary curvature in a right coronary artery through CT imaging and Caro et al. [5] also demonstrated the common carotid arteries are curved with the radius of curvature 10D by PC-MR angiography. Many other studies showed notably higher secondary curvatures in various vasculatures qualitatively [9, 12, 13].

To investigate effects of pulsatile inflow, canonical flow rate waveform [4] that was derived from in vivo measurement in common carotid and normalized by mean flow rate was imposed at the inlet of the tube as shown in Fig. 2. The mean Reynolds number Re based on mean velocity U and vessel diameter D was 350, which matches representative physiological conditions in common carotid arteries [4]. Another scaling parameter for pulsatile flow, Womersley number, defined as $\mathrm{Wo} = 0.5D\sqrt{2\pi f/\nu}$, where f is the cardiac frequency and ν is the kinematic viscosity of the blood was 4.0 in this study. For all cases, unsteady fully developed velocity profiles derived from Womersley solution in rigid pipe was imposed as inflow velocity boundary conditions. No slip and zero pressure conditions were applied on the vessel wall and on the outlets, respectively.

2.2 Computational fluid dynamics

Three-dimensional unsteady incompressible momentum and continuity equations for Newtonian fluid flow were solved as

$$\rho\frac{\partial \mathbf{u}}{\partial t} + \rho\mathbf{u}\cdot\nabla\mathbf{u} = -\nabla p + \nabla\cdot\mathbf{T}, \tag{2}$$

$$\nabla\cdot\mathbf{u} = 0, \tag{3}$$

where $\mathbf{u}$ and p is fluid velocity vector and pressure, respectively. The stress tensor $\mathbf{T}$ is defined as

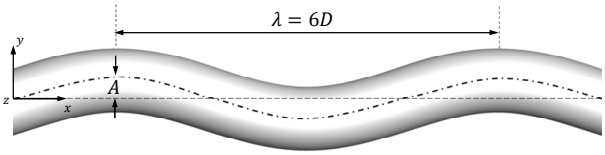

Fig. 1. Geometry of sinusoidally wavy vessel.

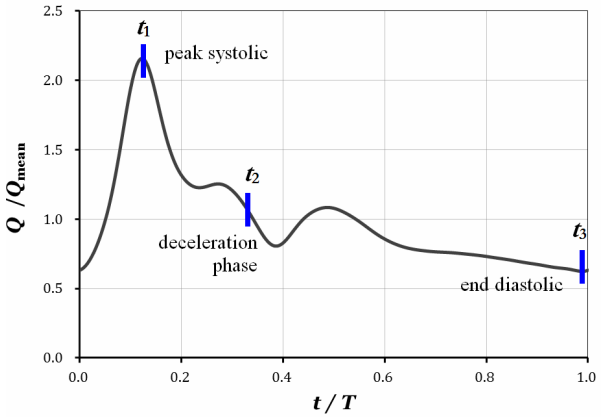

Fig. 2. Pulsatile flowrate waveform for inflow boundary condition.

$$\mathbf{T} = \mu\left(\nabla\mathbf{u} + \nabla\mathbf{u}^T\right). \tag{4}$$

Non-Newtonian rheology of blood is known to have only minor effect on global hemodynamic characteristics in relatively high Reynolds number within large normal vessel [14, 15].

In numerical technique, the Galerkin finite element method based on iso-parametric P2-P1 Taylor-Hood tetrahedral elements [16-18] was used to solve Eqs. (2) and (3). The convective terms were decoupled from the unsteady Stokes equations using a second-order operator-integration-factor time-splitting approach [16] and integrated by a direct Lagrangian integration method. Stokes equations were solved using a preconditioned conjugate-gradient Uzawa method.

Each CFD model was discretized finely into approximately 1400000 quadratic tetrahedral elements. Each simulation was run for three cardiac cycles to ensure fully developed flow and damp out initial transients and the data from simulation of the third cardiac cycle are used for analysis.

2.3 Particle tracking

To quantify the mixing performance in a sinusoidally wavy tube, it is necessary to trace their positions with initial seeding of differently color-labeled particles. In the present study, 60000 massless passive particles are initially distributed at the inlet of the fluid domain. Fig. 3 shows the initial distribution of two species of particles, black and grey particles, at the vessel inlet. The black and grey particles are seeded in such a way that the black particles are distributed near the wall and the grey particles are located near the center of the vessel. The number of black and grey particles is set to be equal. It conse-

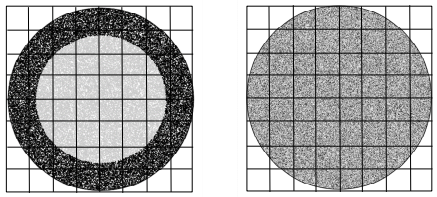

Fig. 3. Initial particle distribution at the inlet of the vessels and perfect mixing overlaid with grid.

quently leads to the same areas of black and grey particles if we assume that the particles are generated uniformly. Then, the position of particles throughout fluid domain was traced by numerically integrating the following advection equation, based on unsteady flow field for a cardiac cycle obtained by CFD simulations.

$$\frac{d\mathbf{x}}{dt} = \mathbf{u}(\mathbf{x}, t). \tag{5}$$

Here, **x** is the position vector of the particle in Cartesian coordinates and **u** is velocity which is a function of space and time. The equation was integrated in time by applying the Runge-Kutta method.

2.4 Quantification of mixing degree

Previously, mixing behavior caused by helical tube was visualized by using numerical and experimental techniques for tracking fluid particle trajectory [19].

However, this was merely qualitatively demonstrated by comparing visualization of secondary flow and particle trajectories at specific cross section between numerical and experimental results. In another study for chaotic micromixers, a formulation of entropy mixing measure was introduced to quantify mixing degree by obtaining the position of different color labeling particle in cross sections [20]. This entropic measure of mixing was also used to quantify of mixing performance induced by helical geometries with various curvatures [11]. However, this study considered only steady flow condition.

In the present study, we considered time-varying pulsatile flow condition, which is intrinsic in cardiovascular flow within sinusoidally wavy tube.

Here, we briefly introduce the formulation and technique for calculation of entropy to be interpreted as a measure of particle mixing. Generally, entropy can be interpreted as a tendency of a process or an expression of disorder of randomness. Thus, non-uniformity or an increasing disorder leads to an increasing in entropy value. Formulation for calculating mixing entropy was introduced in Ref. [20] as

$$S = \sum_{i=1}^{N_c} w_i \sum_{k=1}^{N_s} n_{i,k} \log n_{i,k}. \tag{6}$$

Here, N_c and N_s are the total number of the cell and the species, respectively. w_i is the weighting factor defined in such way that w_i is zero if there is no particle in the cell or there are only particles with single color inside the cell. For the cells in which there are both black and grey particles, w_i is one. $n_{i,k}$ is the particle number fraction of the k^{th} species in the i^{th} cell. In the present study, we used N_c = 14400 for the cell and N_s = 2 for the species. Since the entropy S itself does not have an adequately physical meaning, an alternative property, relative entropy κ, is introduced.

$$\kappa = \frac{S - S_0}{S_{max} - S_0}, \tag{7}$$

where S_0 is minimum mixing entropy at the inlet, S_{max} is uniform mixing state where maximum entropy mixing can be obtained. From Eq. (7), greater mixing or a better mixing performance indicates an increasing of κ. In particular, κ = 1 indicates ideal perfect mixing where black and grey particles totally mix together and κ = 0 is the case that there is no mixing occurs. Note that the relative entropy only exists meaningfully at appropriate number of cells, and comparing the values of relative entropy between different cases has a physical meaning only when the same number of counting cells was considered. As a result, we kept the same number of counting cells for whole studies.

3. Results and discussion

3.1 Axial velocity fields

Axial velocity distributions on various cross-sections at two different time points in a cardiac cycle including peak systolic ($t = t_1$) and deceleration phase ($t = t_2$) (ref. Fig. 2) are shown in Figs. 4 and 5, respectively. At the peak systolic phase, when the amplitude of sinusoidal vessel is small, which is the case of A = 0.1D, axial velocity profile resembles the one of straight pipe, that is, parabolic distribution with maximum velocity at the center. However, as the amplitude of the vessel increases, velocity profiles change to the crescent shape, which is typical velocity profile (Dean flow) in a curved pipe. Axial velocity peak alternately skewing upward or downward the vessel wall depending on the slice position is evidently shown in higher amplitude vessel. On the other hand, somewhat peculiar velocity profiles were observed at the deceleration phase. For A = 0.1D, the maximum velocity region in elliptic shape was located at the center of the vessel. However, with increase of the amplitude, crescent shaped velocity profiles were generated, but with facing opposite wall compared to the one in normal Dean flow. Similar velocity patterns were observed in *in vivo* measurement of individual human carotid artery flow by PC-MR imaging [21]. It may be inferred that such velocity patterns are caused by periodic varying of curvature. Moreover, comparisons of velocity pattern at two pair sections A-A, C-C and B-B, D-D (Fig. 5) visually revealed

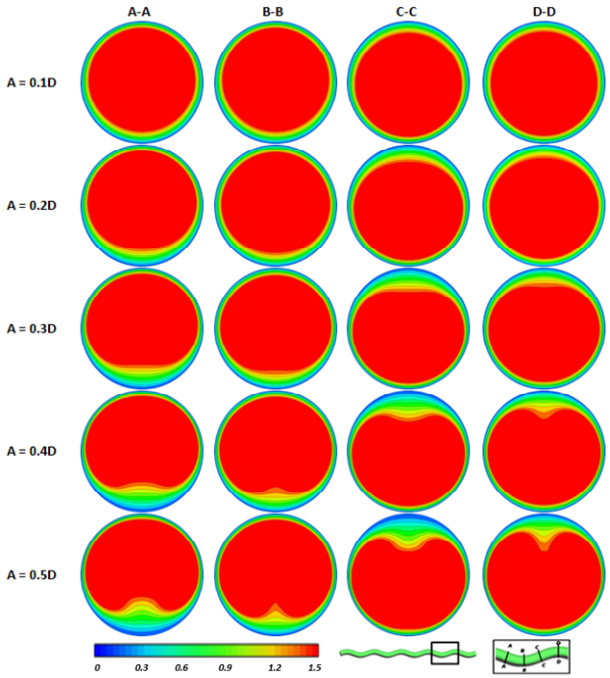

Fig. 4. Axial velocity contours at the peak systolic phase.

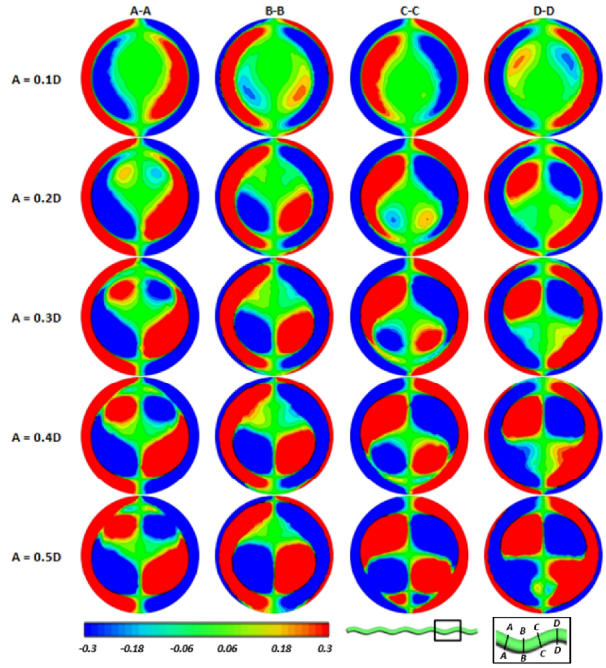

Fig. 6. Axial vorticity contours at the peak systolic phase.

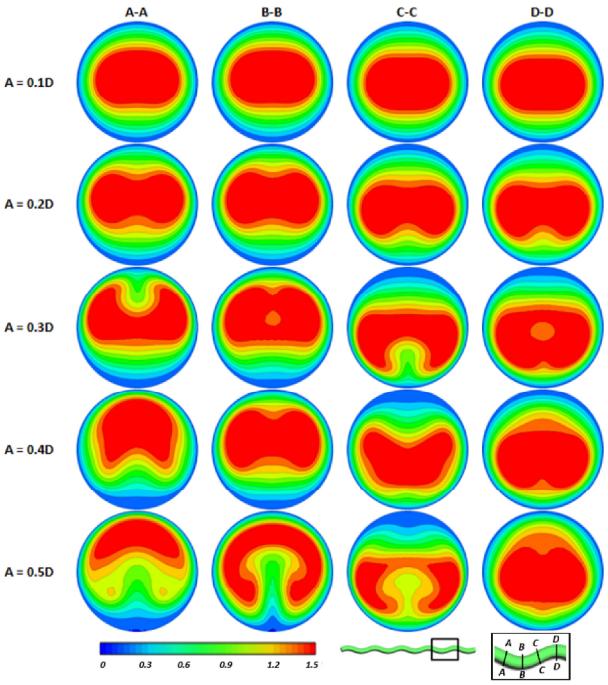

Fig. 5. Axial velocity contours at the deceleration phase.

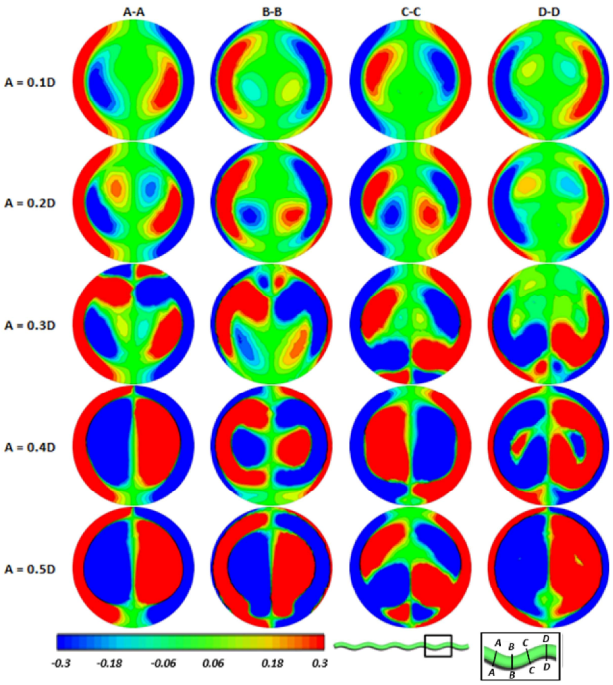

Fig. 7. Axial vorticity contours at the deceleration phase.

that velocity is relatively unstable and still developing in the cases of the amplitude beyond 0.4D.

3.2 Streamwise vorticity

Considering temporal influence on the behavior of vorticity at an interest section such as A-A in Figs. 6-8, vortices in the core becomes weakened as time goes from systolic to diastolic phase and only a weak vortex pair remains at the diastolic phase. Similar behavior was obtained in two stronger vortices near the wall. During periodic cardiac cycle, vorticity at the same section mostly keeps its profile while its magnitude tends to decline due to reducing inflow rate.

Moreover, it was demonstrated that four dominant vortices

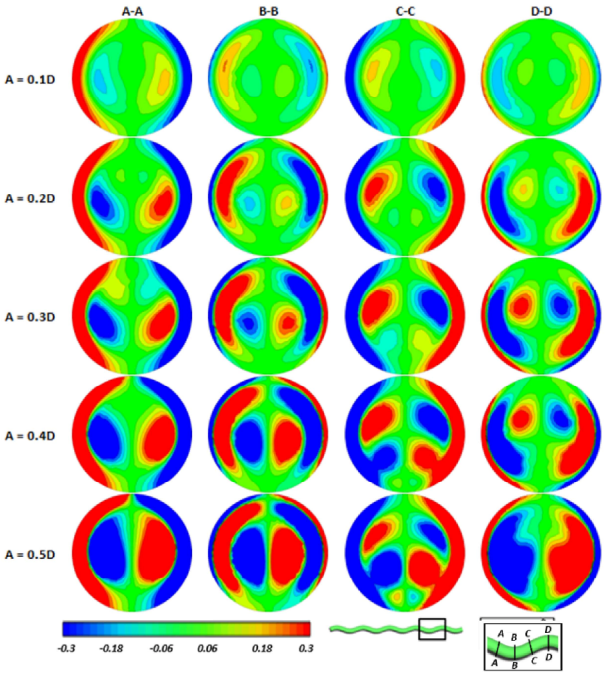

Fig. 8. In-plane velocity contours and streamtraces at the end diastolic phase.

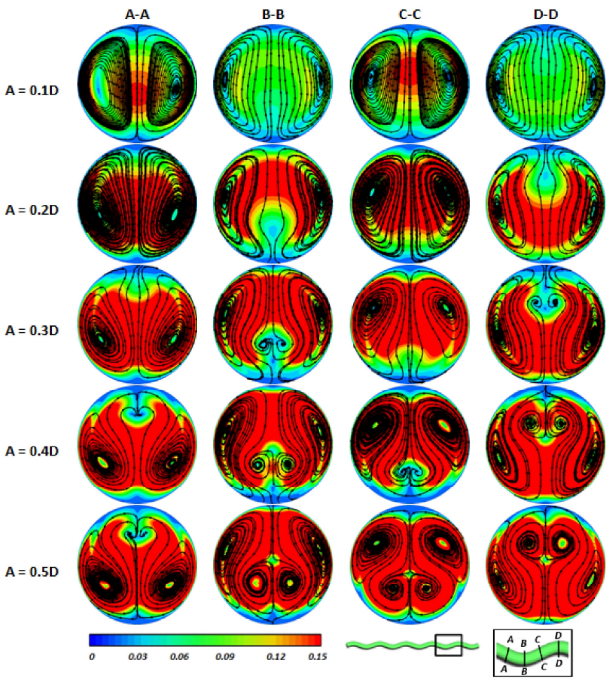

Fig. 9. In-plane velocity contours and streamtraces at the peak systolic phase.

are created when the amplitude is above A = 0.4D, although there are only two dominant (single counter-rotating pair) vortices in lower amplitude cases. The difference of vorticity contours in the symmetric pair of cross-sections in axial direction (A-A & C-C, and B-B & D-D) at higher amplitude cases than A = 0.3D indicates the flow is not fully developed.

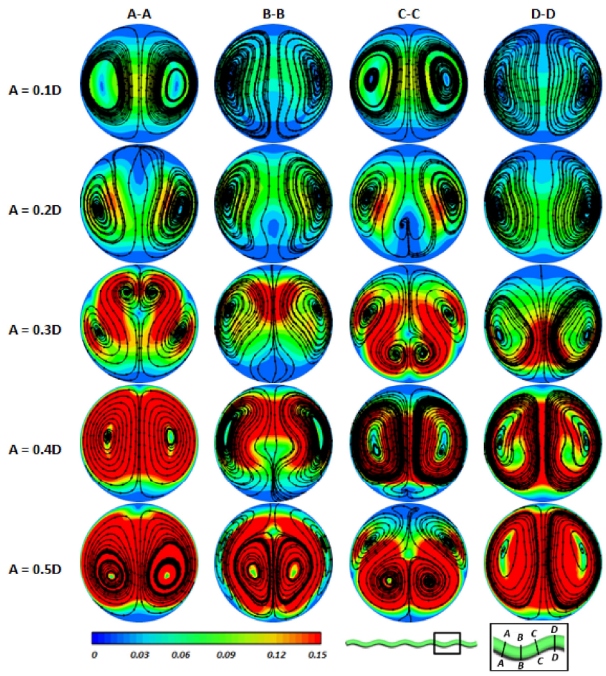

Fig. 10. In-plane velocity contours and streamtraces at the deceleration phase.

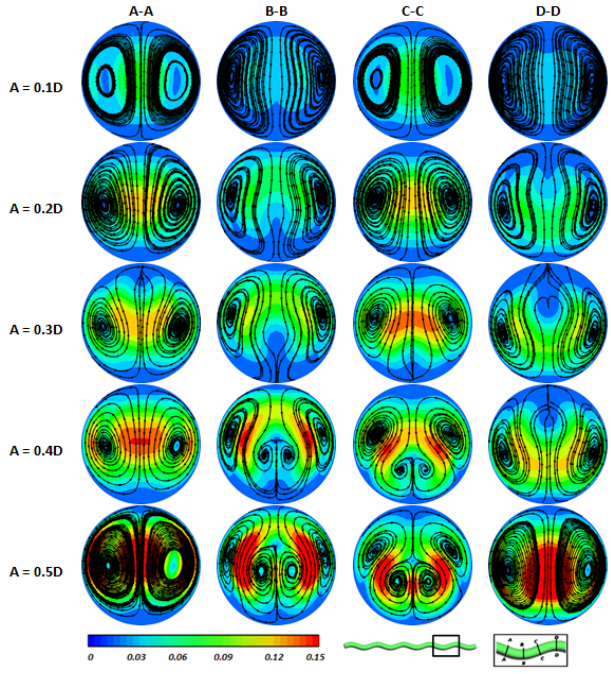

Fig. 11. In-plane velocity contours and streamtraces at the end diastolic phase.

3.3 In-plane velocity and streamtraces

In-plane velocity magnitude profile overlaid by streamtraces in the in-plane reference is shown in Figs. 9-11 at three different time points. The in-plane velocity can be calculated as

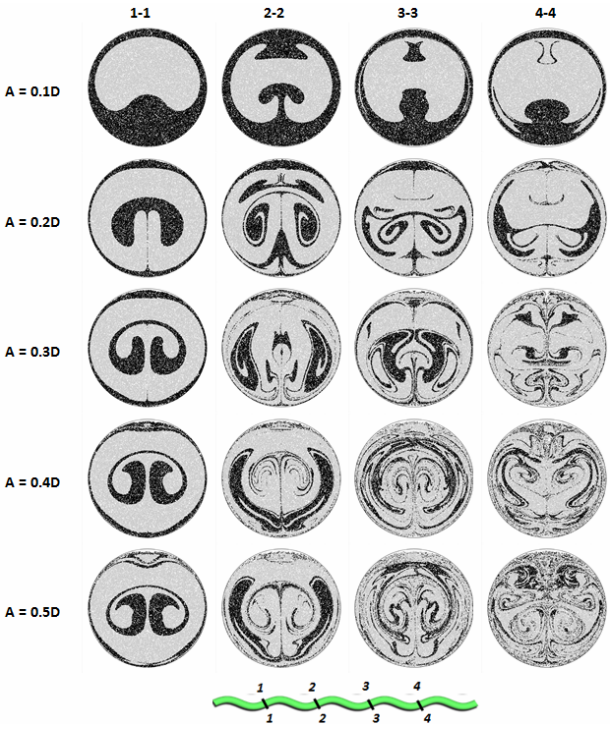

Fig. 12. Particle mixing for various sinusoidal amplitudes at the deceleration phase.

$$V_{inplane} = V_{Cartesian} - V_{translation}, \tag{8}$$

where $V_{translation}$ can be derived by taking the derivative of the geometric equation of sinusoidal wavy centerline with respect to time [11]. Vortical structures are clearer in streamtrace plot. In all pitch-length sections, two counter-rotating symmetric vortices are evident in the case of lower amplitude than A = 0.3, but additional pairs of counter-rotating vortices are evolved with higher vessel amplitude. Since particle trajectories generally correspond to the streamtrace patterns from Figs. 9-11, considerable particle mixing would be expected by the simple sinusoidal wavy tube with relatively small amplitude.

Streamtrace patterns in Figs. 9-11 also show that increasing curvature of vessel leads to produce four vortices with stronger intensity instead of only two vortex in case of A = 0.1D.

3.4 Mixing characteristics

Fig. 12 shows distribution of colored particles at four subsequent pitch-length sections for sinusoidal tubes with various amplitudes. Initially, 60000 particles are seeded uniformly on the inlet surface. In the case of A = 0.1D, due to the small amplitude of the vessel, axial velocity profile skewed toward the wall slightly. Hence, only small amount of black particles near the wall came into the core even at four pitch downstream location of x = 24D (Sec. 4.4) and mixing occurred very little. Higher curvature vessel induced stronger mixing behavior by secondary flow with more distorted particle distribution pattern between two kinds of species. In case of A = 0.3D, after only three pitch length, most of black particle rapidly moved into the core and mixed with grey particles. Comparing mixing at downstream location of x = 24D (Sec. 4.4), it is clear that considerable amount of mixing occurs in case of higher amplitude than A = 0.3D. The degree of mixing is apparently higher than that of helical pipe in steady flow shown in Cookson et al. [11]. The strongest mixing in which black particles strongly mingled grey particles was found in the case of A = 0.5D. However, for all cases, very little mixing was observed at one pitch length.

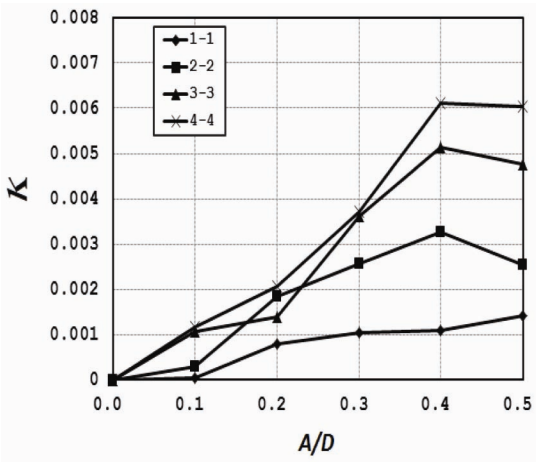

Fig. 13. Relative entropy κ as the measure of mixing for various sinusoidal amplitude.

The pattern of black particles also reveals a good agreement with the in-plane velocity profile. In case of A = 0.1D, according to Figs. 9-11, the vorticity pattern shows that there are merely two vortices dominant in in-plane frame for the whole periodic cycle. However, in a vessel with higher curvature beyond A = 0.3D, it is easily realized that besides two dominant vortices near the wall, another smaller vortex pair in the core obviously observed.

To quantify the degree of mixing, the normalized mixing entropy was calculated as shown in Fig. 13. The results clearly showed that relative entropy κ increases and mixing becomes stronger with each pitch length. At the first pitch length (Sec. 1.1), small value of κ indicates a minor mixing at this section even in the vessel with high amplitude. Magnitude of κ becomes greater in sequence of pitch along the vessel and keeps increasing gradually as amplitude of curvature increases up to A = 0.4D. In the range beyond this amplitude, the value of κ stays similar or is even lower despite increasing amplitude of sinusoidal tube. These mixing effects by relatively small amplitude wavy geometry of the vessel may suspend activation of particle adhesion and red blood cell aggregation.

3.5 Wall shear stress

In Fig. 14, Wall shear stress (WSS) distributions with different amplitude of sinusoidally shaped vessel are presented.

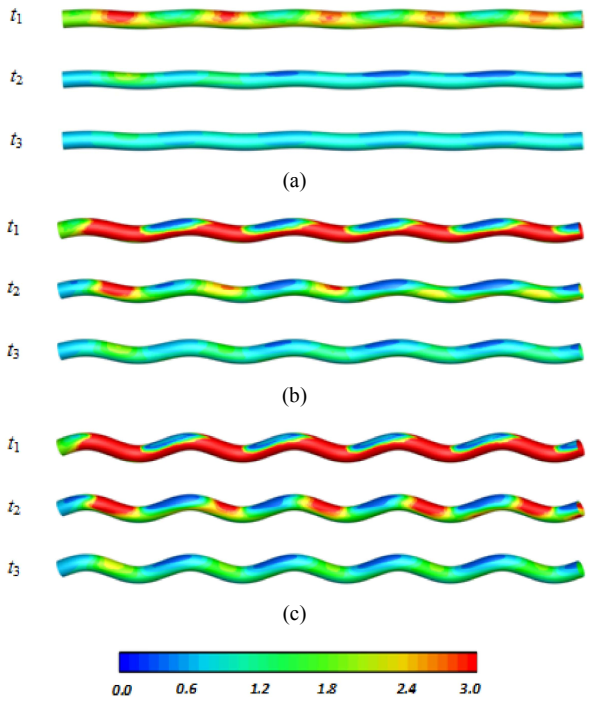

Fig. 14. Comparison of normalized WSS distribution: (a) A = 0.1D; (b) A = 0.3D; (c) A = 0.5D.

The WSS was normalized by that of the Poiseuille flow with the mean Reynolds number in the straight tube with constant radius.

The skewed peak axial velocity core to the wall by the secondary flow results in the asymmetric WSS distribution in a cross-section. WSS patterns are similar regardless of the amplitude of vessel and temporal phase in a cardiac cycle with alternating high and low WSS profile along the axis of vessel, which is different than in helical shaped pipe where twisted ribbon shaped WSS distribution was exhibited [22]. In the vessel of the amplitude A = 0.3D, the WSS is more than two times greater at the heel and 50% lower at the toe of the sinuous vessel than the one in the straight tube. This trend is more extended to higher than four folds in larger amplitude vessel, in particular at the deceleration phase. This implies that the real in vivo WSS distributions are more complex than axisymmetric ones calculated based on presumptive parabolic velocity profile, even in seemingly normal and straight vessel.

4. Conclusions

The present numerical study of pulsatile flow within sinusoidally wavy vessel revealed that there is significant effect on the nature of flow patterns and particle mixing behavior by small amplitude secondary curvature of vessel geometry. This implies that characterizing accurate geometry is essential in accurate prediction of in vivo hemodynamics and may motivate further study on any possibility of reflection of secondary flow on vascular remodeling and pathophysiology.

Acknowledgment

This work was supported by Institute for Information & communications Technology Promotion (IITP) grant funded by the Korea government (MSIP) (No.R0101-15-0171).

References

[1] C. G. Caro, J. M. Fitz-Gerald and R. C. Schroter, Arterial wall shear and distribution of early atheroma in man, *Nature*, 223 (1969) 1159-1161.

[2] A. M. Malek, S. L. Alper and S. Izumo, Hemodynamic shear stress and its role in atherosclerosis, *JAMA*, 282 (21) (1999) 2035-2042.

[3] M. H. Friedman, O. J. Deters, F. F. Mark, C. B. Bargeron and G. M. Hutchins, Arterial geometry affects hemodynamics. A potential risk factor for atherosclerosis, *Atherosclerosis*, 46 (2) (1983) 225-231.

[4] S.-W. Lee, L. Antiga, J. D. Spence and D. A. Steinman, Geometry of the carotid bifurcation predicts its exposure to disturbed flow, *Stroke*, 39 (8) (2008) 2341-2347.

[5] C. G. Caro, C. L. Dumoulin, J. M. Graham, K. H. Parker and S. P. Souza, Secondary flow in the human common carotid artery imaged by MR angiography, *J. of Biomechanical Engineering*, 114 (1) (1992) 147-149.

[6] M. Ford, Y. J. Xie, B. A. Wasserman and D. A. Steinman, Is flow in the common carotid artery fully developed?, *Physiological Measurement*, 29 (11) (2008) 1335-1349.

[7] J. G. Myers, J. A. Moore, M. Ojha, K. W. Johnston and C. R. Ethier, Factors influencing blood flow patterns in the human right coronary artery, *Annals of Biomedical Engineering*, 29 (2) (2011) 109-120.

[8] P. Tortoli, V. Michelassi, G. Bambi, F. Guidi and D. Righi, Interaction between secondary velocities, flow pulsation and vessel morphology in the common carotid artery, *Ultrasound in Medicine & Biology*, 29 (3) (2001) 407-415.

[9] P. M. O'Flynn, E. T. Roche and A. S. Pandit, Generating an ex vivo vascular model, *ASAIO J.*, 51 (4) (2005) 426-433.

[10] L. Goubergrits, K. Affeld, J. Fernandez-Britto and L. Falcon, Geometry of the human common carotid artery. A vessel cast study of 86 specimens, *Pathology - Research and Practice*, 198 (8) (2002) 543-551.

[11] A. N. Cookson et al., Mixing through stirring of steady flow in small amplitude helical tubes, *Annals of Biomedical Engineering*, 37 (2009) 710-721.

[12] D. Gallo, D. A. Steinman and U. Morbiducci, An insight into the mechanistic role of the common carotid artery on the hemodynamics at the carotid bifurcation, *Annals of Biomedical Engineering*, 43 (1) (2015) 68-81.

[13] N. B. Wood, S. Z. Zhao, A. Zambanini, M. Jackson, W. Gedroyc, S. A. Thom, A. D. Hughes and X. Y. Xu, Curvature and tortuosity of the superficial femoral artery: a possible risk factor for peripheral arterial disease, *J. of Applied Physiology*, 101 (5) (2006) 1412-1418.

[14] S.-W. Lee and D. A. Steinman, On the relative importance

of rheology for image-based CFD models of the carotid bifurcation, *J. of Biomechanical Engineering*, 129 (2) (2007) 273-278.

[15] S.-W. Lee, On the effect of shear-thinning rheology on hemodynamic characteristics in basilar tip aneurysms with implication of two distinct flow patterns, *JMST*, 26 (10) (2012) 3125-3132.

[16] C. Ethier, D. A. Steinman and M. Ojha, Comparisons between computational hemodynamics, photochromic dye flow visualization and magnetic resonance velocimetry, *The haemodynamics of arterial organs-comparisons of computational predictions with in vivo and in vitro data,* Edited by X. Y. Xu and M. W. Collins, WIT Press (1999) 131-183.

[17] C. Ethier, S. Prakash, D. A. Steinman, R. Leask, G. Couch and M. Ojha, Steady flow separation patterns in a 45 degree junction, *J. of Fluid Mechanics,* 411 (2000) 1-38.

[18] P. Minev and C. Ethier, A characteristic/finite element algorithm for the 3-D Navier-Stokes equations using unstructured grids, *Computer Methods in Applied Mechanics and Engineering*, 178 (1998) 39-50.

[19] K. Yamamoto, A. Aribowo, Y. Hayamizu, T. Hirose and K. Kawahara, Visualization of the flow in a helical pipe, *Fluid Dynamics Research*, 30 (4) (2002) 251-267.

[20] T. G. Kang and T. H. Kwon, Colored particle tracking method for mixing analysis of chaotic micromixers, *J. of Micromechanics and Microengineering*, 14 (2004) 891-899.

[21] A. K. Wake, Modeling fluid mechanics in individual human carotid arteries, *Ph.D. Thesis*, Georgia Institute of Technology (2005).

[22] K. E. Lee, J. S. Lee and J. Y. Yoo, A numerical study on steady flow in helically sinuous vascular protheses, *Medical Engineering & Physics*, 33 (2011) 38-46.

M. T. Nguyen received his M.S. in Mechanical Engineering from the University of Ulsan, Korea in 2012. Currently, he is a Ph.D. candidate in Mechanical Engineering at the University of Ulsan. His research interests include computational fluid dynamics, biomedical engineering and high performance computing.

S.-W. Lee received his Ph.D. in Mechanical Engineering from the University of Illinois at Chicago in 2005. Currently, he is an associate professor of Mechanical Engineering at the University of Ulsan. His research interests include cardiovascular mechanics and computational fluid dynamics.